UNIVERZITA KOMENSKÉHO V BRATISLAVE

FAKULTA MATEMATIKY, FYZIKY A INFORMATIKY

Mgr. Zuzana Kučerová

Autoreferát dizertačnej práce

Spectrometer and Kinematic Studies for New Physics Searches in Rare $K^+ \to \pi^+ \nu\overline{\nu}$ Decay at NA62 Experiment at CERN

na získanie akademického titulu *philosophiae doctor*

v odbore doktorandského štúdia: 1124 Jadrová a subjadrová fyzika

BRATISLAVA, 2020

Dizertačná práca bola vypracovaná v dennej forme doktorandského štúdia na
Katedre teoretickej fyziky
Fakulty matematiky, fyziky a informatiky
Univerzity Komenského v Bratislave.

Predkladateľ: Mgr. Zuzana Kučerová
Katedra teoretickej fyziky
Fakulta, matematiky, fyziky a informatiky
Univerzity Komenského
Mlynská dolina
842 48 Bratislava

Školiteľ: doc. RNDr. Tomáš Blažek, PhD.
Katedra teoretickej fyziky
FMFI UK Bratislava

Konzultant: Mgr. Michal Kovaľ, PhD.
Karlova Univerzita, Praha

Študijný odbor: 1124 Jadrová a subjadrová fyzika

Predseda odborovej komisie:

prof. RNDr. Jozef Masarik, DrSc.
Katedra jadrovej fyziky a biofyziky
Fakulta, matematiky, fyziky a informatiky
Univerzity Komenského
Mlynská dolina
842 48 Bratislava

Abstract

The LHC experiments have already reached their energy limitations and are starting high luminosity programs to continue direct searches for new physics signals. At the same time the importance of low energy experiments in the field of experimental particle physics is rising, as they offer a wide range of possibilities to challenge the Standard Model of particle physics and to look for indirect signs of new physics in quantum corrections and forbidden processes.

The NA62 experiment at CERN is one of the most active particle experiments in the kaon physics today. It was designed specifically to study the ultra-rare "golden decay" $K^+ \to \pi^+\nu\overline{\nu}$ ($K_{\pi\nu\nu}$). A new result with the most precise measurement of the $K_{\pi\nu\nu}$ branching fraction obtained from the full NA62 data set recorded in 2016–2018, has been recently presented at the ICHEP 2020 conference. The same data is used in multiple other analyses of rare kaon decays and searches for new particles from the hidden sector, also producing world leading results.

NA62 is preparing for the new run expected to start in 2021. Analysis of the available data set showed that the NA62 has potential to reach the precision of the Standard Model $K_{\pi\nu\nu}$ branching fraction prediction. Additionally, it revealed several drawbacks of the current experimental setup and indicated data analysis methods and algorithms that need improvement before the new run.

This work details the author's contribution towards the $K_{\pi\nu\nu}$ decay measurement at the NA62. The contribution is twofold, which is reflected in the organization of the presented thesis.

First the analysis of the STRAW spectrometer reconstruction efficiency for single track events is presented. The efficiency is measured for π^+, μ^+ and e^+ tracks from selected $K^+ \to \pi^+\pi^0$, $K^+ \to \pi^0\mu^+\nu_\mu$ and $K^+ \to \pi^0 e^+\nu_e$ events, respectively. The track reconstruction efficiency for all three types of charged tracks is measured to be above 95 % in 2016 and above 98 % in 2017 and 2018 data sets when all reconstructed candidates are considered. The efficiency for tracks reconstructed using hits from all four STRAW chambers is above 92 % in 2016 and above 94 % in 2017 and 2018. The reconstruction efficiency measured on π^+ tracks was used in the $K_{\pi\nu\nu}$ analysis of 2017 and 2018 data sets.

Secondly, one of the critical parts of the $K_{\pi\nu\nu}$ analysis – the matching between the kaon and pion tracks – is studied. A new matching algorithm based on hypothesis testing using likelihood is proposed. Performance of the algorithm is studied with fully reconstructed $K^+ \to \pi^+\pi^+\pi^-$ event candidates and decrease in mismatch rate of up to

80 % is observed. Additionally, a part of the main $K_{\pi\nu\nu}$ analysis was implemented independently in this work to study the effect of the proposed matching algorithm on the reconstruction tails of the two dominant kaon decay background sources, $K^+ \to \pi^+\pi^0$ and $K^+ \to \mu^+\nu$, in the 2017 data. The new algorithm significantly improves the resolution tails of the kinematic variable m^2_{miss} and thus reduces the $K^+ \to \pi^+\pi^0$ background by up to 30 %, leading to an increased signal-over-background ratio with a single event sensitivity comparable to the main analysis. After the planned upgrade of the NA62 detector system, the new matching algorithm is intended to be used in the main $K_{\pi\nu\nu}$ analysis in the next run.

Keywords: NA62 experiment, rare kaon decays, reconstruction efficiency, likelihood

1 $K^+ \to \pi^+ \nu\overline{\nu}$ decay

Decay of the charged kaon to a pion and a neutrino-antineutrino pair ($K_{\pi\nu\nu}$) is one of the most promising processes to challenge the Standard Model (SM) predictions. Leading contributions to the $K_{\pi\nu\nu}$ amplitude in the SM are governed by one-loop electroweak processes [1], as shown in Figure 1.1. Due to the large top mass, the amplitude is dominated by the top quark loops, but receives also sizeable contribution from the charm transitions [2]. The low energy hadronic matrix elements corresponding to quark currents between hadron states can be extracted from well measured $K \to \pi l \nu_l$ decays. The branching fraction can be predicted very accurately with the largest uncertainty coming from features inherent to perturbative QCD. The latest SM prediction reads [3]

$$\mathcal{B}\left(K^+ \to \pi^+ \nu\overline{\nu}\right)(\text{SM}) = (8.4 \pm 1.0) \times 10^{-11}. \tag{1.1}$$

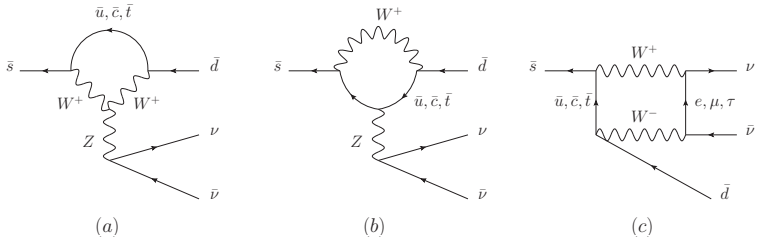

Figure 1.1: Feynman diagrams for $K^+ \to \pi^+ \nu\overline{\nu}$ leading contributions [4].

The NA62 Experiment at CERN approaches the $K^+ \to \pi^+ \nu\overline{\nu}$ measurement with a high momentum (75 GeV/c) unseparated hadron beam with the kaon component decaying in flight [1]. The overall goal of NA62 is to measure the branching fraction of the $K_{\pi\nu\nu}$ decay at 10 % precision level.

The experimental signature of a $K_{\pi\nu\nu}$ event is one incoming kaon decaying into a single positively charged pion and missing energy carried away by neutrinos. Two signal regions with minimal contamination from the common kaon decays are defined using the kinematic variable squared missing mass

$$m^2_{miss} = \left(P_{K^+} - P_{\pi^+}\right)^2, \tag{1.2}$$

where P_{K^+} is the four-momentum of the detected upstream beam particle identified as a kaon and P_{π^+} is the four-momentum of the charged particle detected downstream, identified as a pion. The choice of the signal regions shown in Figure 1.2 provides 90 % kinematic rejection of other K^+ decays, listed in Table 1.1. Seven other regions are used in the $K_{\pi\nu\nu}$ analysis: three peak and four control regions for background estimation. To reduce the probability of wrongly reconstructing m^2_{miss} due to misreconstruction

of kaon or pion momenta, two additional variables, $m^2_{miss}(RICH)$ and $m^2_{miss}(beam)$, are computed and further constrain mainly the signal regions. For evaluation of $m^2_{miss}(RICH)$, the track momentum in P_{π^+}, measured by the downstream spectrometer (STRAW), is replaced with the momentum measured in RICH while keeping the original direction. In $m^2_{miss}(beam)$, the GTK (beam spectrometer) momentum in P_{K^+} is replaced with the run-dependent mean beam momentum measured with $K_{3\pi}$ events.

Additionally, each region is divided into four π^+ momentum bins: (15–20) GeV/c, (20–25) GeV/c, (25–30) GeV/c and (30–35) GeV/c.

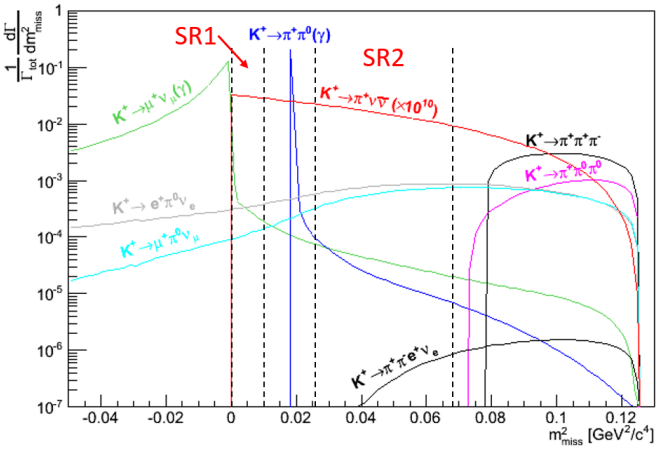

Figure 1.2: Differential branching fraction as a function of the kinematic variable m^2_{miss} (Equation (1.2)). Two signal regions are indicated by dashed lines.

Final state	Abbreviation	Branching fraction
$\mu^+\nu_\mu$	$K_{\mu 2}$	$63.56 \pm 0.11\%$
$\pi^+\pi^0$	$K_{2\pi}$	$20.67 \pm 0.08\%$
$\pi^+\pi^+\pi^-$	$K_{3\pi}$	$5.58 \pm 0.02\%$
$\pi^0 e^+\nu_e$	K_{e3}	$5.07 \pm 0.04\%$
$\pi^0\mu^+\nu_\mu$	$K_{\mu 3}$	$3.35 \pm 0.03\%$
$\pi^+\pi^0\pi^0$	$K_{3\pi^0}$	$1.76 \pm 0.02\%$
$\pi^+\pi^- e^+\nu_e$	K_{e4}	$(4.25 \pm 0.02) \times 10^{-5}$
$\pi^+\gamma\gamma$		$(1.01 \pm 0.06) \times 10^{-6}$
$\pi^+\nu\bar{\nu}$	$K_{\pi\nu\nu}$	$(8.4 \pm 1.0) \times 10^{-11}$

Table 1.1: K^+ decay modes relevant for the presented thesis. Standard abbreviations and branching fractions [5] are listed. SM prediction for the $K_{\pi\nu\nu}$ branching fraction is quoted [3].

The NA62 Experiment collected three data sets for the $K_{\pi\nu\nu}$ decay measurement, denoted by the year of data taking (2016–2018). Separate blind analyses were adop-

ted in each recorded data set. The 2017 $K_{\pi\nu\nu}$ analysis is of great importance for the presented thesis. Specifically, the matching between the kaon and pion tracks, crucial for the reconstruction of signal events and suppression of background contribution to the $K_{\pi\nu\nu}$ signal regions, is studied on the 2017 data and discussed in Section 3. Optimization of the matching algorithm is desired for the future $K_{\pi\nu\nu}$ analysis to lower the background from the $K_{2\pi}$ and $K_{\mu 2}$ reconstruction tails and potentially also from upstream events.

Process	Events expected
$K^+ \to \pi^+\nu\bar{\nu}$ (SM)	$2.16 \pm 0.13_{\text{syst}} \pm 0.26_{\text{ext}}$
$K^+ \to \pi^+\pi^0(\gamma)$	$0.29 \pm 0.03_{\text{stat}} \pm 0.03_{\text{syst}}$
$K^+ \to \mu^+\nu(\gamma)$	$0.15 \pm 0.02_{\text{stat}} \pm 0.04_{\text{syst}}$
$K^+ \to \pi^+\pi^- e^+\nu$	$0.12 \pm 0.05_{\text{stat}} \pm 0.06_{\text{syst}}$
$K^+ \to \pi^+\pi^+\pi^-$	$0.008 \pm 0.008_{\text{syst}}$
$K^+ \to \pi^+\gamma\gamma$	$0.005 \pm 0.005_{\text{syst}}$
$K^+ \to \pi^0\ell^+\nu$ $(\ell = \mu, e)$	< 0.001
Upstream background	$0.89 \pm 0.24_{\text{stat}} \pm 0.20_{\text{syst}}$
Total background	$1.46 \pm 0.25_{\text{stat}} \pm 0.21_{\text{syst}}$

(a)

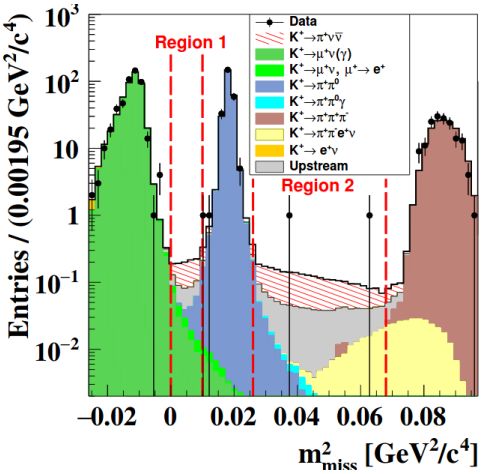

(b)

Figure 1.3: (a): Summary of the expected numbers of the $K_{\pi\nu\nu}$ decays and background events in the $K_{\pi\nu\nu}$ signal regions in the 2017 data set. The upstream, $K_{2\pi}$, $K_{\mu 2}$ and $K_{3\pi}$ contributions were estimated from data, the rest was estimated from simulation. (b) Reconstructed m^2_{miss} (Equation (1.2)) distribution of data events passing the $K_{\pi\nu\nu}$ event selection from the 2017 data set. The expected background and SM $K_{\pi\nu\nu}$ event contributions are superimposed as stacked histograms. The distributions of the $K_{2\pi}$, $K_{\mu 2}$ and $K_{3\pi}$ decays and of the upstream events are extracted from data. The other contributions are obtained from simulations [6].

Two $K_{\pi\nu\nu}$ candidate events were observed in the 2017 data set. The expected number of Standard Model $K_{\pi\nu\nu}$ events and the background contribution to the $K_{\pi\nu\nu}$ signal regions are summarized in Figure 1.3a. The background is dominated by upstream decays in the beam line and interactions between the beam particles and upstream subdetectors, with significant contribution from $K_{2\pi}$ and $K_{\mu 2}$ kinematic tails, as shown in Figure 1.3b.

Additionally, one $K_{\pi\nu\nu}$ candidate event was observed in signal region 2 in the 2016 data set, and 17 $K_{\pi\nu\nu}$ candidate events in total were observed in the 2018 data set. Combination of the results leads to the total of $\sim$10 expected SM signal events and $\sim$7 expected background events, while observing 20 events. This results in the new

measurement of the $K_{\pi\nu\nu}$ branching fraction:

$$\mathcal{B}(K^+ \to \pi^+ \nu\overline{\nu}) = \left(11.0^{+4.0}_{-3.5}\big|_{\text{stat.}} \pm 0.3_{\text{syst.}}\right) \times 10^{-11}. \tag{1.3}$$

The analysis of the full NA62 data set showed that a significant improvement of the upstream background suppression and increase of the $K_{\pi\nu\nu}$ signal acceptance are needed. With the aim of achieving this, the NA62 collaboration plans to install an additional station to the beam spectrometer and a new upstream veto counter before resuming the data taking in 2021. Subsequently, certain cuts used to suppress upstream background in the current analysis are going to be relaxed.

2 STRAW track reconstruction efficiency

The efficiency is measured separately using three different kaon decay modes: $K_{2\pi}$, $K_{\mu 3}$ and K_{e3}. The data recorded using a minimum-bias trigger which does not include STRAW spectrometer is used for the efficiency measurement. Three offline selection procedures are developed to select $K_{2\pi}$, $K_{\mu 3}$, and K_{e3} events without using STRAW information.

Each event selection starts with π^0 identification by selecting cluster pairs in the electromagnetic calorimeter (LKr) to be considered as $\pi^0 \to \gamma\gamma$ decay candidates. For each pair of selected clusters, a vertex is found numerically using a constraint on the invariant mass of the two photon candidates and the (X, Y) position of the vertex, which is given by the beam (kaon) path. Given the cluster energies, their positions in the LKr and the reconstructed vertex position, the π^0 four-momentum is calculated as the sum of the four-momenta of the two photon candidates.

The $K_{2\pi}$ event selection is based on the identification of π^+ using calorimeters and the background suppression using muon and photon vetoes. Additionally, a cut on the π^+ invariant mass variable is applied to select a clean $K_{2\pi}$ sample.

The $K_{\mu 3}$ selection is based on the muon pointer reconstruction using information from the RICH, the muon identification in the MUV3, and photon rejection using the LAV and the SAV sub-detectors. Finally, a cut on a squared missing mass variable is applied to select the sample entering the efficiency evaluation.

In the K_{e3} selection the LKr information is used to reconstruct the e^+ pointer energy, while the radius and the position of the corresponding RICH ring are used for positron identification.

Each selection algorithm produces a pointer representing the predicted position and momentum of the positively charged track (π^+, μ^+, or e^+). They are used as inputs to the efficiency evaluation algorithm. The pointer is propagated from the vertex position downstream in the magnetic fields of the Blue Tube and the MNP33 magnet. Events that enter the evaluation of the STRAW track reconstruction efficiency are required to have their pointer in the geometrical acceptance of all four STRAW chambers; the distance from the beam axis is required to be above 10 cm. For each reference pointer, a STRAW candidate compatible with the pointer is looked for. The pointer position and its momentum are compared to the reconstructed STRAW candidates at the $Z = 180\,\mathrm{m}$ plane, i.e. the candidate reference position before the MNP33 magnet. It is required that the momentum difference between the pointer and a STRAW candidate is less than 5 GeV/c (10 GeV/c) for π^+ and e^+ (μ^+) pointers. Furthermore, a momentum dependent cut is imposed on the distance between the pointer and a STRAW candi-

date. If a matching candidate is found, the event is considered efficient and enters the numerator of the efficiency.

The track reconstruction efficiency in a run is calculated as a ratio of the number of efficient events and the number of all events with a pointer in the geometrical acceptance of four STRAW chambers:

$$\varepsilon = \frac{\text{N efficient events}}{\text{N events with good pointer}}. \tag{2.1}$$

The efficiency dependence on the pointer momentum, position before magnet at $Z = 180\,\mathrm{m}$, distance from beam axis and the instantaneous beam intensity is calculated.

Two classes of inefficient events are identified:

- events with no STRAW candidate reconstructed in the event,
- events with STRAW candidate(s) reconstructed, but no candidate satisfies the position and momentum criteria.

The STRAW reconstruction algorithm is based on hit clustering and produces two types of candidates (tracks). The candidates of the first type are reconstructed using hit information from all four STRAW chambers, while the candidates of the second type miss information from one of the chambers. The momentum and slope measurement resolution are worse for the latter type. Therefore, some of the NA62 analyses, including the main $K^+ \to \pi^+\nu\bar{\nu}$ analysis, do not use the 3-chamber tracks. Track reconstruction efficiency is evaluated by considering both types of candidates and then separately by considering only the 4-chamber tracks.

The STRAW track reconstruction efficiency affects the acceptance of signal and normalization selections in the $K_{\pi\nu\nu}$ analysis and thus enters the evaluation of the single event sensitivity of the $K_{\pi\nu\nu}$ measurement. The efficiency measurement carried out by the author uses minimum bias data samples obtained in 2016, 2017 and 2018 runs.

2.1 Results

The results of the Straw spectrometer reconstruction efficiency measurement are summarized for single track kaon decay events, see Table 2.1. The efficiency is evaluated separately for all tracks ($\geq$3 CH) and for four-chamber tracks (4 CH).

We observe a difference between the 2016 data sample and the 2017+2018 data samples; the efficiency is lower by about 3 % in 2016. The efficiency improvement at the beginning of 2017 was most probably achieved thanks to an upgrade of the STRAW readout firmware. Otherwise, the reconstruction efficiency was stable for all 3 types of studied tracks during the whole data taking period.

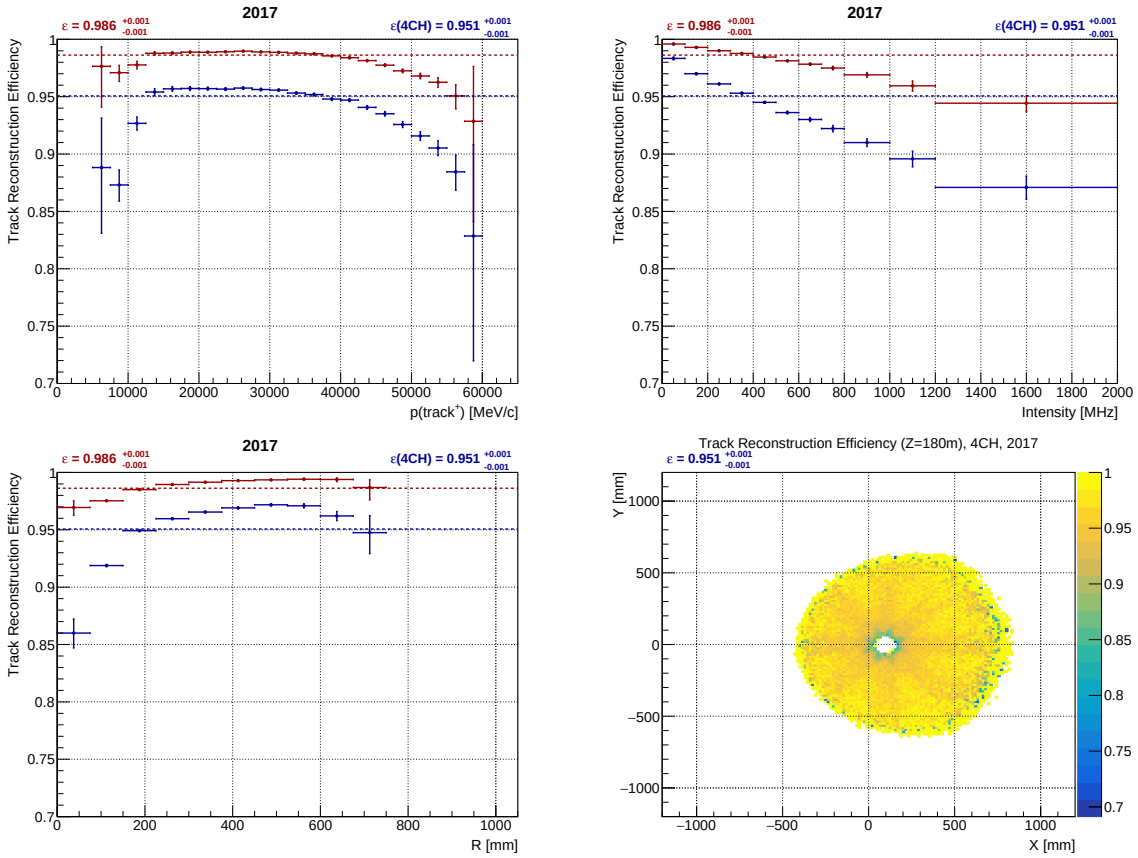

Figure 2.1: π^+ track reconstruction efficiency as a function of the momentum of the reconstructed π^+ pointer (top left), the instantaneous beam intensity (top right), the distance from the beam axis (bottom left), and as a function of the reconstructed π^+ pointer position before the STRAW magnet at $Z = 180\,\mathrm{m}$ (bottom right). Only candidates reconstructed from hits in all four chambers are used for the last. Data sample: 2017, minimum-bias trigger, $K_{2\pi}$ event candidates.

The measured efficiency values in 2017–2018 are above 98 % for all three studied charged particles. The standard efficiency measurement does not take into account events in which a charged particle is lost either due to its decay before or between the STRAW chambers or due to an interaction with the material of the spectrometer, since such events generally do not pass our event selections and thus do not enter the denominator of the efficiency computation as discussed in subsection 2.2.

2.2 Spectrometer track reconstruction efficiency using MC truth

A study is carried out with the standard MC samples without any added pile-up. The goal of this study is to evaluate the intrinsic inefficiency of the Spectrometer candidate reconstruction, as well as to estimate the effect of particle decay and interaction on the candidate reconstruction efficiency. MC truth information is used to select events in

	π^+		μ^+		e^+	
	$\geq$3 CH	4 CH	$\geq$3 CH	4 CH	$\geq$3 CH	4 CH
2016 data	95.7 %	93.3 %	95.8 %	92.8 %	96.5 %	95.2 %
2017 data	98.6 %	95.1 %	98.9 %	94.3 %	99.8 %	98.4 %
2018 data	98.5 %	94.9 %	98.8 %	94.0 %	99.7 %	98.2 %
$K_{2\pi}$ MC	99.7 %	97.4 %				
$K_{\mu 3}$ MC			99.7 %	96.0 %		
K_{e3} MC					99.8 %	97.6 %

Table 2.1: Summary of the Spectrometer track reconstruction efficiency measurement for data and MC. The statistical uncertainties of the presented central values are at the level of 0.2 % or smaller. Results are stable within 0.2 % (0.3 % in 4 CH case) under variation of selection cuts.

the denominator of the efficiency and the true charged track is used as the pointer for the efficiency evaluation. A reconstructed candidate with momentum within 1 GeV/c from the pointer momentum and with a distance from the pointer position in any STRAW chamber smaller than 25 mm is looked for. Events, in which at least one such candidate is found, enter the numerator of the efficiency.

We only consider events in which the charged particle reaches the first STRAW chamber and its position is in the acceptance of all four STRAW chambers. In case the particle decays or interacts inelastically before passing through the fourth chamber, the position is obtained by extrapolation from the latest available MC checkpoint. The fractions of such events are given in Table 2.2.

Decay	Reach end of CH4	Decay in CH1-4	Inelastic[1] interaction in CH1-4
$K_{2\pi}$	97.32%	2.20%	0.48%
$K_{\mu 3}$	99.97%	0.03%	0.00%
K_{e3}	99.95%	0.00%	0.05%

Table 2.2: Probabilities for the charged particle entering the STRAW (in acceptance of all chambers) to reach the end of STRAW CH4, to decay and to interact inellastically.

First, the track reconstruction efficiency is evaluated for particles that reach the end of STRAW CH4. The results in Table 2.3 show that the reconstruction efficiency is lower (especially for K_{e3}) than the efficiency obtained using the standard procedure

[1]Inelastic, Scintillation, Annihilation processes in GEANT4.

	π^+		μ^+		e^+	
	ε [%]	ε(4CH) [%]	ε [%]	ε(4CH) [%]	ε [%]	ε(4CH) [%]
All events	98.84%	96.03%	99.35%	94.91%	95.95%	89.04%
Selected events	99.68%	98.82%	99.88%	97.96%	99.65%	97.91%

Table 2.3: Spectrometer reconstruction efficiency with MC truth.

in Table 2.1. To explain this discrepancy, we evaluated the efficiency on MC events passing the $K_{2\pi}$, K_{e3} and $K_{\mu 3}$ event selections. Results are given in the second row of Table 2.3 and show that for those events, the MC truth efficiency is compatible with the standard results. This can be explained by the fact that the inefficiency in the first MC truth sample is caused by events in which the charged tracks lost significant fraction of their energy or scattered in the STRAW chambers. As a result, they do not pass the selection criteria, especially the kinematic constraints on $m(\pi^+)$ or m^2_{miss}.

3 Kinematic studies for the $K^+ \to \pi^+ \nu\overline{\nu}$ measurement

The second goal of this thesis is to develop a new algorithm for matching single STRAW candidates with GTK candidates. The aim is to improve the performance of the existing algorithm in the $K_{\pi\nu\nu}$ analysis on the 2017 data set with regards to $K_{2\pi}$ and $K_{\mu 2}$ backgrounds. For this project, four event selections ($K_{\pi\nu\nu}$, $K_{2\pi}$ for normalization, $K_{2\pi}$, $K_{\mu 2}$) as well as the standard matching algorithm were implemented independently of the main analysis, but using same selection criteria [6]. Event-by-event comparison of the independent analyses proved to be useful to debug the main 2017 $K_{\pi\nu\nu}$ analysis before opening control and signal regions.

The strategy to develop a new matching algorithm follows three steps. First the $K_{3\pi}$ decay events, in which full kinematic information (momenta and positions of all the decay products) is available, are used to find the correct GTK candidate. Then a new algorithm to match individual pion tracks to GTK candidates is developed, based on standard statistical classification methods involving Bayes' theorem and likelihood-ratio hypothesis testing [7]. The proposed matching algorithm checks compatibility of the reference STRAW track with a subset of reconstructed GTK candidates. Each track-GTK candidate pair is characterized by a set of three values: distance at vertex D_{vtx}, and positive and negative linear combinations of the differences between the RICH and KTAG times associated to the STRAW track and time of the GTK candidate, ΔT_+ and ΔT_-, respectively. Based on these values, two hypotheses are tested. *Kaon* hypothesis H_0, by which the GTK candidate is the correct one and corresponds to the reference downstream track, and *pile-up* hypothesis H_1, by which the GTK candidate is a pile-up particle and does not correspond to the reference downstream track. For each hypothesis, probability density functions of D_{vtx}, ΔT_+ and ΔT_- are provided by fitting the relevant distributions obtained from $K_{3\pi}$ data events in the first step. The event category N is determined by counting the number of GTK candidates of good quality which are compatible with the kaon beam and in time with the STRAW track. Given the category N, the probability f_N of reconstructing and randomly selecting the correct GTK candidate in an event with N good GTK candidates in time with the track is obtained from $K_{3\pi}$ selected events.

The probability that the tested GTK candidate is in fact the correct one corresponding to the reference track is computed as follows:

$$P\left(H_0|\gamma\right) = \frac{\mathcal{L}\left(\gamma|H_0\right) \cdot f_N}{\mathcal{L}\left(\gamma|H_0\right) \cdot f_N + \mathcal{L}\left(\gamma|H_1\right) \cdot \left(1 - f_N\right)}, \tag{3.1}$$

where γ = {D_{vtx}, ΔT_+, ΔT_-} corresponds to a set of values characterizing each track-GTK candidate pair and $\mathcal{L}\left(\gamma|H_i\right)$ is likelihood of H_i given observed set of values γ.

All GTK candidates considered for the reference STRAW track are sorted by decreasing probability, with the best candidate being the one with the largest $P(H_0|\gamma)$. The best GTK candidate is matched to the reference track if the probability is greater than a predefined threshold. In event categories with more than one GTK candidate considered in matching to the reference track (i.e. $N > 1$), the two best GTK candidates are compared using likelihood ratio test

$$\Lambda(\Gamma) = \frac{\mathcal{L}(\Gamma|H_A)}{\mathcal{L}(\Gamma|H_B)}, \tag{3.2}$$

in which $\Gamma = \{\gamma_{c_1}, \gamma_{c_2}\}$ is a set of values obtained by two independent measurements for GTK candidates c_1 and c_2, respectively, and hypothesis H_A corresponds to the case in which the best GTK candidate is the correct one and the second best GTK candidate is a pile-up candidate, and vice versa for hypothesis H_B. Instead of using $\Lambda(\Gamma)$, which is unbounded from above and always equal to or greater than 1, a new function is defined with the same monotonicity and codomain equal to interval [0, 1):

$$\mathcal{F}(\Gamma) = \frac{\Lambda(\Gamma) - 1}{\Lambda(\Gamma)}. \tag{3.3}$$

Finally, the thresholds for $\mathcal{F}(\Gamma)$ and the probability of the best GTK candidate (separately in categories $N = 1$ and $N > 1$) are obtained by a histogram scanning procedure in comparison with the standard matching algorithm. Two variables of interest, the total number of expected $K_{2\pi}$ and $K_{\mu 2}$ events in the $K_{\pi\nu\nu}$ signal regions, $N_{exp\,bg}$, and the number of $K_{2\pi}$ normalization events in the $K_{2\pi}$ peak region, $N_{2\pi N}$, are evaluated from the full $K_{\pi\nu\nu}$ analysis and two ratios are defined:

- $R_{bg} = \big(N_{exp\,bg}(likelihood)\big) \,/\, \big(N_{exp\,bg}(standard)\big)$,
- $R_{2\pi N} = (N_{2\pi N}(likelihood)) \,/\, (N_{2\pi N}(standard))$.

Five sets of thresholds with best performance given by $R_{bg} \leq 1$ and $R_{2\pi N} \geq 1$ are selected and summarized in Table 3.1a.

Performance of the new matching algorithm is first tested with $K_{3\pi}$ events selected from 2017A data set. For each selected event, a $K_{3\pi}$ kaon candidate is built from the three pion candidates. One of the two positive pions is randomly chosen and used as a reference track in the tested STRAW–GTK matching algorithm. Three variables are defined to evaluate the performance by comparing the GTK candidates selected by STRAW–GTK and $K_{3\pi}$– GTK matching algorithms and the results are summarized in Table 3.1b.

Variables A and B are used to assess the performance of the matching algorithm on events in which the correct GTK candidate is reconstructed. They estimate the rates of

	$N=1$	$N>1$	
	$P(H_0\|\gamma)$	$\mathcal{F}(\Gamma)$	$P(H_0\|\gamma)$
SET 1	0.894	0.840	0.636
SET 2	0.952	0.360	0.660
SET 3	0.946	0.396	0.752
SET 4	0.936	0.810	0.714
SET 5	0.930	0.906	0.654

(a)

	A [%]	B [%]	C [%]
Standard	73.47	1.41	2.81
SET 1	79.20	0.44	3.36
SET 2	75.42	1.43	2.61
SET 3	74.19	1.12	2.52
SET 4	74.86	0.45	2.68
SET 5	75.45	0.28	2.81

(b)

Table 3.1: (a) Five sets of threshold values selected by the scanning procedure defining final quality cuts in the new matching algorithm. (b) Comparison of the performance of the new and standard STRAW–GTK matching algorithms evaluated on the same sample of $K_{3\pi}$ events.

good match and mismatch, respectively. Variable C gives an insight into the behavior of the matching algorithm when dealing with upstream background, as it corresponds to the fraction of $K_{3\pi}$ events with only out-of-time GTK candidates reconstructed in the event.

The overall goal is to keep the number of events with incorrectly selected GTK candidate (B and C) as low as possible while retaining the acceptance (given by the sum of events of types A and B) and high good-match rate (A). In the $K_{\pi\nu\nu}$ analysis, the incorrect matching between STRAW and GTK candidates leads to a wrong value of the reconstructed m^2_{miss}. This, in turn, leads to an enlarged background event rate in the signal regions and thus decreases the statistical power of the $K_{\pi\nu\nu}$ branching fraction measurement. Additionally, the acceptance of the matching algorithm is reflected in the overall acceptance of the $K_{\pi\nu\nu}$ event selection.

Comparison with the standard matching algorithm in Table 3.1b shows that the new algorithm can lower the mismatch rate (B) by up to 80 % (relative) and improve the good-match rate (A) by 1 % to 8 % at the same time. The rejection power of events in which the matched GTK candidate corresponds to a pile-up particle is estimated by the column C. The performance varies between different sets of cut values; from 20 % degradation in SET 1 to 10 % improvement in SET 3 with respect to the standard algorithm.

Since the $K_{\pi\nu\nu}$ analysis suffers from low signal acceptance due to strict selection criteria, a matching algorithm with an improved acceptance (and low mismatch rate) is desirable. As expected and also indicated by Table 3.1b, a significant increase in good-match rate (A) in SET 1 results in substantially worsened fake-match rate (C).

This could be an issue in the $K_{\pi\nu\nu}$ analysis where the fake-match rate directly affects the level of upstream background. However, in future data taking at NA62, multiple changes in the experimental setup are planned, aiming at decreasing the upstream background level. Thanks to the improved performance, the new matching algorithm is intended to replace the currently used one in the main analysis of future data.

Performance of the STRAW–GTK matching algorithm in the $K_{\pi\nu\nu}$ analysis can be judged by multiple criteria. The focus of this work is on the $K_{2\pi}$ and $K_{\mu 2}$ backgrounds from non–gaussian reconstruction and radiative tails of the corresponding m^2_{miss} distributions, which span across the $K_{\pi\nu\nu}$ signal regions. Backgrounds result from $K_{2\pi}(\gamma)$ and $K_{\mu 2}(\gamma)$ events which pass the $K_{\pi\nu\nu}$ event selection and are reconstructed in the $K_{\pi\nu\nu}$ signal regions. This only occurs when all photons (from π^0 decay and radiative) remain undetected, and in case of $K_{\mu 2}$, the muon is wrongly identified as a pion. Such events enter the signal regions due to misreconstruction of m^2_{miss} mainly caused by multiple scattering or pattern recognition error in the reconstruction procedures in GTK or STRAW, or by an incorrect STRAW–GTK matching.

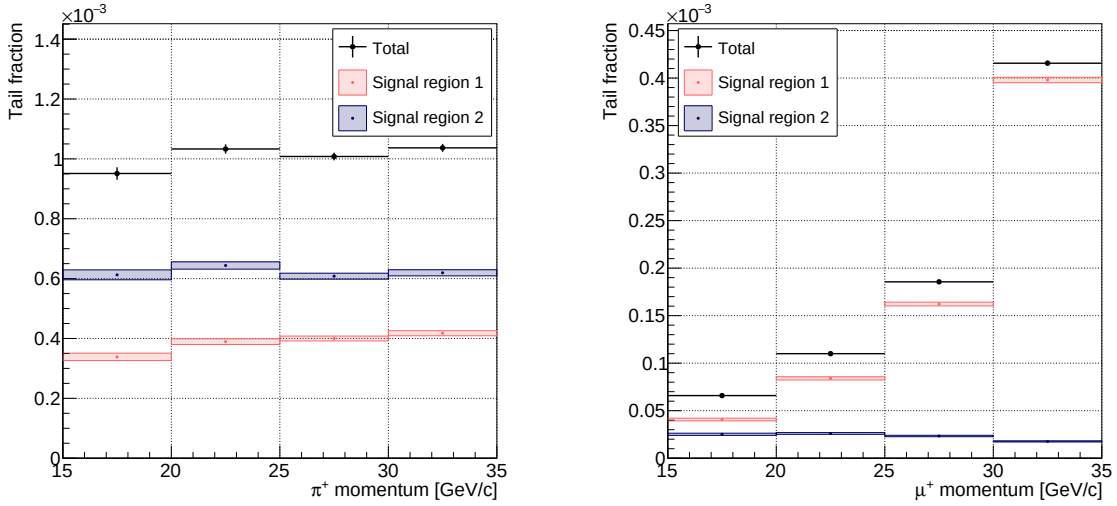

Figure 3.1: $K_{2\pi}$ and $K_{\mu 2}$ tail fractions in both $K_{\pi\nu\nu}$ signal regions measured with the likelihood matching algorithm (SET 5) on the full 2017 data set. Tail fractions are evaluated in four bins of the π^+ or μ^+ track momentum.

The backgrounds are estimated with dedicated $K_{2\pi}$ and $K_{\mu 2}$ event selections applied on data. While the estimation of $K_{\mu 2}$ tails includes both components, the radiative part in $K_{2\pi}$ event selection is strongly suppressed by π^0 identification and a two-body decay kinematics requirement. Consequently, the effect of the remaining radiative component of $K_{2\pi}$ tails is measured separately in the main $K_{\pi\nu\nu}$ analysis.

The $K_{2\pi}$ and $K_{\mu 2}$ tail fractions measured on the full 2017 data set in four momentum bins are quantified in Table 3.2. Comparison of the $K_{2\pi}$ tail fraction in signal region 1,

obtained with the standard and likelihood matching algorithms, reveals an improvement of up to 30 % in all momentum bins. Less dramatic improvement (up to 4 %) is observed for the $K_{2\pi}$ tail fraction in signal region 2 for three of the selected sets of thresholds for the likelihood matching algorithm. Up to 12 % (6 %) worsening is seen for the $K_{\mu 2}$ tail fraction in the signal region 1 (2), mainly in the high momentum bin. Nevertheless, lower $K_{2\pi}$ tail fraction in signal region 1 is enough to produce smaller (by more than 8 % at the best) total expected background for three of the five proposed sets.

	$f^{\rho}_{kin,2\pi}$ [$\times 10^{-4}$]		$f^{\rho}_{kin,\mu\nu}$ [$\times 10^{-4}$]		$A(\pi\nu\nu)$	$A(2\pi N)$	SES	$\frac{N_{exp\ \pi\nu\nu}}{N_{exp\ bg}}$
	SR1	SR2	SR1	SR2	[%]	[%]	[$\times 10^{-10}$]	
Standard	5.502	6.443	2.015	0.216	2.454	6.563	0.389	4.881
SET 1	4.533	6.651	2.265	0.230	2.481	6.687	0.379	4.853
SET 2	5.378	6.538	2.071	0.218	2.484	6.648	0.382	4.728
SET 3	4.946	6.375	2.034	0.216	2.429	6.507	0.388	4.988
SET 4	4.120	6.207	2.065	0.220	2.400	6.461	0.392	5.291
SET 5	3.957	6.206	2.099	0.222	2.392	6.453	0.393	5.282

Table 3.2: Summary of the obtained results: $K_{2\pi}$ and $K_{\mu 2}$ tail fractions in the $K_{\pi\nu\nu}$ signal regions (summed over momentum bins), acceptances of the $K_{\pi\nu\nu}$ and $K_{2\pi}$ normalization selections computed from the $K_{\pi\nu\nu}$ and $K_{2\pi}$ Monte Carlo samples, respectively; single event sensitivity (SES) measured on the full 2017 data set; the expected signal-over-background ratio (accounting only for the $K_{\mu 2}(\gamma)$ and $K_{2\pi}$ background).

The acceptance of the $K_{\pi\nu\nu}$ event selection with the likelihood matching algorithm varies for the proposed sets of threshold values between up to 1.2 % improvement and about 2.5 % loss with respect to the case with the standard matching. Similar results (up to 1.9 % improvement and less than 1.7 % loss) are observed for the acceptance of the $K_{2\pi}$ normalization selection (see Table 3.2). Both acceptances are used in evaluation of the single event sensitivity and the expected number of $K_{\pi\nu\nu}$ events to be observed in the $K_{\pi\nu\nu}$ signal regions combined, both varying between up to 1 % worsening and up to 3 % improvement. The expected signal-over-background ratio, shown in the last column of Table 3.2, is higher by up to 8.4 %. The ratio reveals that the major part of the improvement comes from the signal region 1 for m^2_{miss} in range (0.005, 0.01) GeV$^2/c^4$ dominated by the left tail of the $K_{2\pi}$ distribution.

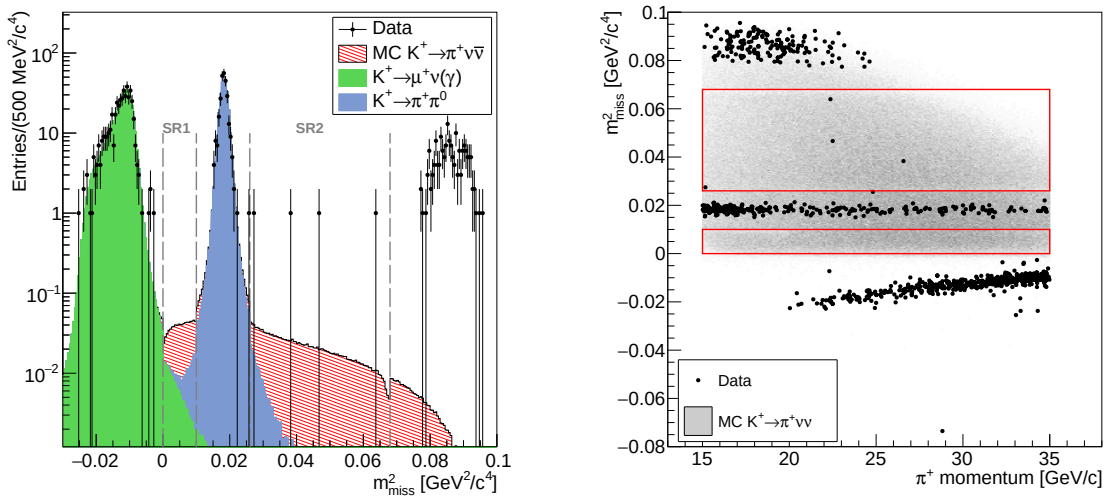

(a) (b)

Figure 3.2: (a) Stack plot obtained as a combination of the m^2_{miss} distribution of the $K_{\pi\nu\nu}$ MC events passing the $K_{\pi\nu\nu}$ selection and two distributions of 2017 data events selected by the $K_{2\pi}$ and $K_{\mu 2}$ selections, overlaid with the $K_{\pi\nu\nu}$– selected data. Distributions are produced with the likelihood matching algorithm (to be compared with Figure 1.3b). Contributions from upstream events, K_{e4}, $K_{3\pi}$, and other less abundant background components are missing. Grey dashed lines indicate the two $K_{\pi\nu\nu}$ signal regions. (b) m^2_{miss} distribution of events passing the $K_{\pi\nu\nu}$ event selection with the likelihood matching algorithm, as a function of the π^+ track momentum (to be compared with Figure 23 in [6]). Grey area corresponds to the $K_{\pi\nu\nu}$ Monte Carlo events, black dots are 2017 data events. Two red rectangles correspond to the $K_{\pi\nu\nu}$ signal regions. The final cuts of the likelihood matching algorithm are defined by threshold values of SET 5.

Figure 3.2 shows the 2017 data and $K_{\pi\nu\nu}$ Monte Carlo events passing the $K_{\pi\nu\nu}$ event selection. Three peak regions, corresponding to the three most abundant kaon decays, are recognized in data: $K_{\mu 2}$ at negative m^2_{miss}, $K_{2\pi}$ at $m^2(\pi^0)$ between the $K_{\pi\nu\nu}$ signal regions, and $K_{3\pi}$ at large m^2_{miss}. Data points in the signal regions correspond to the observed $K_{\pi\nu\nu}$ event candidates. The $K_{\pi\nu\nu}$ event selection with both standard and likelihood matching algorithms results in zero events in the signal region 1 and three (or four) $K_{\pi\nu\nu}$ event candidates in the signal region 2, two of which (and only these two) are also observed by the main $K_{\pi\nu\nu}$ analysis [6]. Investigation of the third event revealed that it was rejected by an older version of the `StrawSegmentAlgorithm` tool used in the main $K_{\pi\nu\nu}$ analysis. The extra $K_{\pi\nu\nu}$ candidate event is observed with four out of the five proposed sets of final matching cuts for the likelihood algorithm.

References

[1] NA62 Collaboration. 'Proposal to Measure the Rare Decay $K^+ \to \pi^+ \nu\overline{\nu}$ at the CERN SPS'. 2005.

[2] Andrzej Buras. 'Flavour Dynamics: CP Violation and Rare Decays'. In: *The Subnuclear Series*. Vol. 38. Mar. 2001. DOI: 10.1142/9789812778253_0005.

[3] Andrzej J. Buras et al. '$K^+ \to \pi^+ \nu\overline{\nu}$ and $K_L \to \pi^0 \nu\overline{\nu}$ in the Standard Model: status and perspectives'. In: *JHEP* 11 (2015), p. 033. DOI: 10.1007/JHEP11(2015)033.

[4] Andrzej J. Buras. 'Weak Hamiltonian, CP violation and rare decays'. In: *Les Houches Summer School in Theoretical Physics, Session 68: Probing the Standard Model of Particle Interactions*. June 1998, pp. 281–539. arXiv: hep-ph/9806471.

[5] Particle Data Group. 'Review of Particle Physics'. In: *Progress of Theoretical and Experimental Physics* 2020.8 (Aug. 2020). 083C01. ISSN: 2050-3911. DOI: 10.1093/ptep/ptaa104.

[6] NA62 Collaboration. *An investigation of the very rare $K^+ \to \pi^+ \nu\overline{\nu}$ decay*. 2020. arXiv: 2007.08218 [hep-ex].

[7] Helge Voss. 'Classification'. In: *Data Analysis in High Energy Physics*. John Wiley & Sons, Ltd, 2013. Chap. 5, pp. 153–186. ISBN: 9783527653416. DOI: 10.1002/9783527653416.ch5.

Author's publications

1. Zuzana Kučerová (on behalf of the NA62 Collaboration), *Recent results in kaon physics*, PoS (Beauty2019) 028.
2. Zuzana Kučerová (on behalf of the NA62 Collaboration), *Search for $K^+ \to \pi^+ \nu\overline{\nu}$ at CERN*, J. Phys.: Conf. Ser. 1586 (DISCRETE 2018).
3. Zuzana Kučerová and Michal Koval', *Spectrometer reconstruction efficiency for single track events*, NA62 Internal Note, NA62-20-05, 2020.
4. Eduardo Cortina Gil et al. (NA62 Collaboration), *An investigation of the very rare $K^+ \to \pi^+ \nu\overline{\nu}$ decay*, arXiv: 2007.08218, submitted to JHEP.
5. Eduardo Cortina Gil et al. (NA62 Collaboration), *Search for heavy neutral lepton production in the K^+ decays to positrons*, Phys. Lett. B807: (2020) 135599.
6. Eduardo Cortina Gil et al. (NA62 Collaboration), *First search for $K^+ \to \pi^+ \nu\overline{\nu}$ using the decay-in-flight technique*, Phys. Lett. B791: (2019) 156-166.
7. Eduardo Cortina Gil et al. (NA62 Collaboration), *Searches for lepton number violating K^+ decays*, Phys. Lett. B797: (2019) 1-9.
8. Eduardo Cortina Gil et al. (NA62 Collaboration), *Search for production of an invisible dark photon in π^0 decays*, J. High Energ. Phys. (2019) 182.
9. Eduardo Cortina Gil et al. (NA62 Collaboration), *Search for heavy neutral lepton production in K^+ decays*, Phys. Lett. B778: (2018) 137-145.